

RESEARCH

Open Access



Unveiling gastric precancerous stages: metabolomic insights for early detection and intervention

Xiaoyue Zhang^{1,2}, Ziming Lin^{1,2}, Boyan Xu^{1,2}, Chenyu Ma^{1,2}, Bowen Jiang^{1,2}, Yan Geng³, Yingyue Sheng¹, Yuanyuan Dai¹, Yuzheng Xue^{1*} and Yilin Ren^{1,4*}

Abstract

Background Gastric precancerous lesions (GPL) represent a heterogeneous, multi-stage process that involves transition from a benign to a malignant state. To optimize prevention and intervention strategies, accurate methods must clearly distinguish between precancerous stages and predict progression risks at early stages.

Methods The metabolomic profiles of 188 GPL tissues and matched normal tissues were characterized using ultra-high-performance liquid chromatography-tandem mass spectrometry. Both multivariate and univariate statistical analyses were used to identify metabolomic features differentiating normal, atrophic, and intestinal metaplasia states in the stomach, followed by preliminary functional validation.

Results From experiments conducted on two cohorts, we established a reliable clinical gastric tissue metabolomic map, which clearly distinguished between normal, atrophic, and intestinalized gastric tissues. We then identified metabolic biomarkers that differentiated various GPL stages. Furthermore, key metabolites were validated in in vitro studies. Relative acyl group and glycerophospholipid abundance was higher in normal gastric tissue when compared to GPL, whereas organic acids were more prevalent in precancerous tissues than in normal tissues. A combination of glycerophosphocholine, tiglylcarnitine, malate, sphingosine, and γ -glutamylglutamic acid may serve as powerful biomarkers to distinguish normal tissue from GPL.

Conclusion We used ultra-high-performance liquid chromatography with tandem mass spectrometry to effectively characterize metabolomic profiles in clinical gastric tissue samples. Key metabolites were identified and validated using targeted metabolomics. This study identified the metabolomic profiles of gastric tissues with atrophy and intestinal metaplasia of the gastric mucosa, uncovering and preliminarily validating key metabolites that may be used to assess high-risk populations and diagnose GPL, potentially advancing targeted gastric cancer prevention and treatment efforts.

Keywords Gastritis, Gastric cancer, Gastric precancerous lesions, Biomarkers

*Correspondence:

Yuzheng Xue
yuzhengxue_ahjnu@126.com
Yilin Ren
elyn0108@163.com

¹Department of Gastroenterology, Affiliated Hospital of Jiangnan University, Wuxi 214122, China

²Wuxi School of Medicine, Jiangnan University, Wuxi 214122, China

³School of Life Science and Health Engineering, Jiangnan University, Wuxi 214122, China

⁴Key Laboratory of Industrial Biotechnology of Ministry of Education, School of Biotechnology, Jiangnan University, Wuxi 214122, China



© The Author(s) 2025. **Open Access** This article is licensed under a Creative Commons Attribution-NonCommercial-NoDerivatives 4.0 International License, which permits any non-commercial use, sharing, distribution and reproduction in any medium or format, as long as you give appropriate credit to the original author(s) and the source, provide a link to the Creative Commons licence, and indicate if you modified the licensed material. You do not have permission under this licence to share adapted material derived from this article or parts of it. The images or other third party material in this article are included in the article's Creative Commons licence, unless indicated otherwise in a credit line to the material. If material is not included in the article's Creative Commons licence and your intended use is not permitted by statutory regulation or exceeds the permitted use, you will need to obtain permission directly from the copyright holder. To view a copy of this licence, visit <http://creativecommons.org/licenses/by-nc-nd/4.0/>.

Background

Globally, gastric cancer (GC) is the fifth most common cancer and the third leading cause of cancer-related deaths [1]. Regrettably, the majority of patients receive a diagnosis at advanced or late local stages, leading to poor prognoses [2]. GC develops via a multi-step process, beginning with superficial gastritis and advancing through to chronic atrophic gastritis (AG), intestinal metaplasia (IM), low-grade intraepithelial neoplasia, and high-grade intraepithelial neoplasia, ultimately leading to invasive GC [3, 4]. According to epidemiological data, AG is a prevalent and persistent condition, often without symptoms, affecting over half of the world's population at some stage [5]. IM significantly increases GC risks, doubling the likelihood of its occurrence [6]. Fortunately, at gastritis and IM stages, timely detection and intervention can effectively control or even reverse the disease. However, once the disease has progressed to different intraepithelial neoplasia levels, it is difficult to manage progression with non-surgical treatments [7]. Therefore, identifying high-risk populations at AG and IM stages is crucial for developing and implementing effective prevention and management strategies. While *Helicobacter pylori* (*H. pylori*) infection is strongly associated with gastritis and gastric disease advancement [8, 9], it does not directly cause GC [7]. Currently, limited biomarkers can accurately predict GPL progression. Therefore, to inform precise clinical intervention strategies, addressing GC prevention and control challenges require enhanced etiological research and the exploration of novel molecular features to delineate gastric lesion progression.

A fundamental feature of cancer cells is the reprogramming of energy metabolism, which promotes tumor cell proliferation [10–12]. Metabolic dysregulation significantly contributes to GC development, highlighting the need to characterize metabolic profiles associated with disease progression [13–16]. High-throughput metabolomics technology enables the identification and quantification of endogenous low-molecular-weight metabolites [17, 18], thereby highlighting complex

interactions between the host, genes, and the environment [19]. Thus, metabolomics has become a promising tool for distinguishing GC molecular features and identifying biomarkers [13, 20].

Many studies have investigated GC metabolomic molecular features and core metabolic pathways. Kuligowski et al. used metabolomics to identify tryptophan, kynurenine, and phenylacetylglutamine as potential GC biomarkers, in their plasma metabolomic analysis of over 400 participants [21], Huang et al. showed that α -linolenic acid, linoleic acid, and palmitic acid were significantly associated with IM progression [22]. To our knowledge, most gastritis and IM studies have focused on blood, urine, and other biological samples [22–24], with no direct research on lesion sites. In this study, we conducted a comprehensive metabolomic analysis of 188 clinical tissue samples from 98 patients, focusing on AG and IM stages. Using pseudotargeted metabolomics technology, which provides higher sensitivity and broader dynamic monitoring ranges when compared to untargeted metabolomics [25], we identified differential metabolites between AG, IM, and relatively normal tissues, and explored the metabolic changes from normal to AG and progression to IM.

Materials and methods

Patients and tissue samples

Between April and June 2023, 26 patients from the Department of Gastroenterology at Jiangnan University Affiliated Hospital South Campus, who underwent gastroscopy or treatment, were enrolled for targeted metabolomics analysis. An additional 71 patients were recruited between July 2023 and April 2024 for potential metabolic biomarker verification. Patients were recruited with no history of gastric or other cancers and no other diagnosed specific diseases, including digestive system diseases, prior to sampling. Relatively normal tissue samples (controls) comprised of gastric mucosal tissues taken at 5 cm away from matched lesion sites. Samples were collected by two experienced gastroenterologists during endoscopic procedures, and histological identification was performed by pathologists. The Ethics Committee of Jiangnan University Affiliated Hospital approved the study and all patients provided written informed consent before enrollment. Ethics number for: LS2024300. All patients provided written informed consent before enrollment. The patients' baseline clinical characteristics, including age, sex, and *H. pylori* infection status, are summarized in and Table 1, and the severity grading of *H. pylori* infection is provided in Supplementary Table 4 [26]. Data and software availability pseudotargeted metabolomics data on gastric have been deposited in the European Bioinformatics Institute under accession code MTBLS11835.

Table 1 Clinicopathological characteristics of patients with N, AG and IM in this study

Characteristics	Cohort 1	Cohort 2
Gender (no.)		
Male	13	30
Female	13	41
Age (years, mean \pm SD)	60.77 \pm 9.42	56.79 \pm 11.53
<i>Helicobacter pylori</i> infection status (patients)		
(-)	14	45
(+)	3	9
(++)	3	6
(+++)	3	8

Sample preparation for pseudotargeted metabolomics analysis

Tissue samples were weighed, transferred to 2 mL tubes, and kept on ice. Next, 200 μ L of cold methanol was added, and samples vortexed for 1 min. Two steel beads were added and samples ground at 50 Hz for 10 s; this procedure was performed 3–4 times under low temperature conditions. Samples then underwent 15 min of ultrasonic extraction in an ice bath, followed by centrifugation at $12,000 \times g$ for 15 min at 4 °C. Supernatants (100 μ L) were transferred to new tubes, freeze-dried, and stored at -20 °C. Metabolite extracts were redissolved in 100 μ L of 20% methanol/water prior to Ultra-Performance Liquid Chromatography-Tandem Quadrupole Mass Spectrometry (UPLC-MS/MS).

UPLC-MS/MS conditions for pseudotargeted metabolomics

For metabolite analysis, we used the AB SCIEX Q-Trap 5500 triple quadrupole mass spectrometer (AB SCIEX, USA), using both positive and negative electrospray ionization modes with multiple reaction monitoring scanning. LC separation was performed using an ACQUITY UPLC HSS T3 column (2.1 \times 100 mm, 1.8 μ m) (Waters, USA) for positive ion mode and an ACQUITY UPLC BEH C18 column (2.1 \times 100 mm, 1.7 μ m) (Waters, USA) for negative ion mode. The Exion LC AD system (AB Sciex, USA) featured a binary gradient pump, using 0.1% formic acid in water (solvent A) and acetonitrile (solvent B) as mobile phases at a flow rate of 0.35 mL/min. The gradient started at 5% solvent B, linearly increasing to 99% in 11 min, holding for 2 min, then returning to 5% over the last 2 min. The column temperature was 50 °C and the injection volume was 5 μ L.

MS parameters included an ion source temperature of 550 °C, a curtain gas pressure of 35 psi, a collision gas pressure of 10 psi, and ionspray voltages of 5,500 V in positive mode and -4,500 V in negative mode. Ion gases 1 and 2 were both set to 60 psi. AB SCIEX Analyst 1.7.1 was used to acquire data.

Targeted metabolomics conditions

To create a standard curve, a mixed standard solution containing 1 ppm (1ppm = 1 mg/L) of glycerophosphocholine, sphingosine, malate, and γ -glutamylglutamic acid was prepared and diluted to 1, 5, 10, 50, 100, and 500 ppb (1ppb = 1/1000ppm). A separate tiglylcarnitine dilution series was prepared over the 0.05–10 ppb concentration range. Standard curves were established by plotting analyte-to-internal standard area ratios against concentration. The sample preparation as well as the metabolomics mass spectrometry and chromatographic conditions were consistent with the pseudotargeted metabolomics method, except that the column was ACQUITY UPLC HSS T3 (2.1 \times 100 mm, 1.8 μ m).

Reagents

Methanol (LC-MS grade), acetonitrile, and formic acid were obtained from ThermoFisher Scientific (USA). The 1-methyl-3-nitro-1-nitrosoguanidine (MNNG) (CAS: 70-25-7) and glycerophosphocholine (CAS: 28319-77-9) were sourced from Shanghai Yuanye Bio-Technology Co., Ltd (Shanghai, China). Sphingosine (CAS: 764-22-7), malate (CAS: 97-67-6), and γ -glutamylglutamic acid (CAS: 1116-22-9) were obtained from Shanghai Macklin Biochemical Co., Ltd (Shanghai, China). Tiglylcarnitine (CAS: 64681-36-3) was procured from Shanghai Zhenzhun Bio-Technology Co., Ltd (Shanghai, China).

Cell culture

GES-1 human gastric epithelial cells (iCell Bioscience Inc, Shanghai, China) were cultured to 60% confluence in six-well plates containing Roswell Park Memorial Institute 1640 medium plus 10% fetal bovine serum (FBS) and 1% Penicillin-Streptomycin solution. A humidified environment of 5% CO₂ and 95% air was used to culture cells.

Cell viability assays

Cell viability was assessed using a Cell counting kit-8 (CCK8) kit (Nanjing BEB Laboratories Co., Ltd, Nanjing, China). Cells (8×10^3) were seeded in 96-well plates, allowed to adhere, treated with 1% FBS for 24 h, and exposed to varying metabolite concentrations for another 24 h. Supernatants were then removed, CCK8 solution added, and cells incubated in the dark for 2–4 h. Next, to assess cell viability, the optical density at 450 nm was measured using a SpectraMax 190 light absorption enzyme labeler (Molecular Devices, USA).

Quantitative real-time polymerase chain reaction (qRT-PCR)

Total RNA was isolated from cells by using the TRIzol reagent. qRT-PCR was performed according to the previous protocol [27, 28]. Sequences of the specific primer sets are as follows: *CDX2*: Forward: 5'-TTCCTACAGT CGCTACATCACCA-3', Reverse: 5'-CTGCGGTTCTG AAACCAGATT-3', *KLF4*: Forward: 5'-GTGCCCCGAA TAACAGCTCA-3', Reverse: 5'-TTCTCACCTGTGTG GGTTCG-3', *MUC2*: Forward: 5'-GAGGGCAGAACC CGAAACC-3', Reverse: 5'-GGCGAAGTTGTAGTCG AGAG-3'. Glyceraldehyde-3-phosphate dehydrogenase (GAPDH) was used as a control (Supplement Table 3). The relative gene expressions were analyzed using 2^{- $\Delta\Delta$ CT} method.

Statistical analysis

MetaboAnalyst 6.0 was used for unsupervised principal component analysis and hierarchical data clustering. Samples were normalized for their respective masses to visualize the metabolomic profiles of N, AG and IM

participants. Multivariate analyses, such as partial least squares discriminant analysis (PLS-DA) and the orthogonal partial least squares discriminant analysis (OPLS-DA), were performed to identify key differentiating features between groups. Models were validated using 10-fold cross-validation, with results showing high R^2 and Q^2 values, indicating model reliability, and a permutation testing was performed 200 times to assess the risk of overfitting for the PLS-DA model. Metabolites with Variable Importance in the Projection (VIP) >1 , $p < 0.05$, and Fold Change (FC) >1.5 or <0.5 were selected as differential metabolites. GraphPad Prism 9.4.1 was used for univariate statistical analysis. One-way analysis of variance (ANOVA) with Tukey's post hoc test was applied for multiple group comparisons. An FDR-adjusted p -value threshold of 0.05 was used to assess statistical significance. For two-group comparisons, Student's t -test or the Mann-Whitney U test was applied as appropriate. The data was presented as mean \pm standard error (SEM). $p < 0.05$ was considered statistically significant.

Results

Metabolic profiling of clinical gastric tissue samples

Given limited sample availability (approximately 5 mg), we performed pseudotargeted metabolomics. This approach provides greater sensitivity and a broader dynamic range when compared to non-targeted metabolomics, while eliminating complex feature detection or peak alignment [25].

First, we collected and prepared equal amounts of gastric mucosal tissue samples from clinically N, AG, and IM sites. AG Using UPLC-MS/MS pseudotargeted metabolomics, we identified 433 metabolites across both positive and negative ion modes. To assess instrument stability, we prepared tissue samples with varying concentration gradients and identified 152 and 147 metabolites in positive and negative ion modes, respectively, thereby establishing a database for targeted metabolomics analysis (Supplement Tables 1 and 2).

Metabolic differences between AG, IM, and normal tissues

Pseudotargeted metabolomics was performed on tissue samples ($N=20$, $AG=20$, and $IM=20$) using UHPLC-MS/MS (Table 1, Cohort 1), with the relative quantification of 433 metabolites (Fig. 1A). A PLS-DA score plot showed that IM and Normal groups formed two distinct clusters, with the AG group overlapping to varying degrees with these groups. This observation is consistent with the Correa cascade, in which the disease progresses from N, AG to IM and eventually to gastric cancer (Fig. 2A). Thus, the PLS-DA model demonstrated good reliability, as evidenced by a 10-fold cross-validation yielding high R^2 (0.83) and positive Q^2 (0.57) values (Fig. 2B).

To elucidate metabolic alterations during disease progression, pairwise comparisons between Normal vs. AG, IM, and AG vs. IM were conducted. OPLS-DA supervised analysis identified distinct group separations, revealing distinct metabolic changes as the disease advanced from gastritis to IM (Fig. 2C–E). Using VIP >1 , $P < 0.05$, and FC >1.5 or <0.5 criteria, 18 metabolites were identified (Table 2), including organic acids, four amino acids and derivatives, three lipids, one glycerophospholipid, antibiotics, sphingolipids, and other compounds (Fig. 2F). Fatty acyl groups and glycerophospholipids were more abundant in normal gastric tissue when compared to GPL, whereas organic acids were more prevalent in GPL than in normal tissue. To determine major metabolic and signaling pathways associated with differential metabolites between N, AG, and IM tissues, we performed Kyoto Encyclopedia of Genes and Genomes enrichment analysis, which identified 18 metabolic pathways, encompassing citric acid cycle, pyruvate metabolism, Warburg effects, malate-aspartate shuttle, and pyruvaldehyde degradation pathways (Fig. 2G).

The identification of metabolic biomarkers to differentiate GPL from normal tissue

As differentiating AG from IM tissue was challenging, these groups were merged into a GPL group based on endoscopic observations. Then, a receiver operating characteristic (ROC) curve analysis was conducted on the 18 differential metabolites to evaluate their diagnostic accuracy in distinguishing normal from GPL groups. Of these metabolites, seven had an area under the curve (AUC) value >0.7 , including one with an AUC >0.8 , while the remainder ranged from 0.6 to 0.7 (Supplement Table 5). We cross-referenced this metabolite information and chemical abstracts service (CAS) numbers with the Human Metabolome Database and acquired standards for targeted validation. Ultimately, the following five standards successfully generated calibration curves: glycerophosphocholine, sphingosine, γ -glutamylglutamic acid, tiglylcarnitine, and malate (Fig. 3A–E), and their respective AUC values were 0.801 (95% confidence interval (CI): 0.682–0.920), 0.790 (95% CI: 0.669–0.911), 0.733 (95% CI: 0.592–0.873), 0.719 (95% CI: 0.589–0.849), and 0.665 (95% CI: 0.513–0.817) (Fig. S1A–E). The combined metabolite AUC value was 0.836 (95% CI: 0.714–0.959) (Fig. 3F). These results indicate that the combination of the five metabolites has the potential to serve as potential biomarkers for distinguishing between normal and GPL in gastric tissues.

Metabolic biomarker verification in GPL

To validate the effectiveness of these metabolites, including glycerophosphocholine, as biomarkers distinguishing normal and precancerous gastric tissues, we recruited an

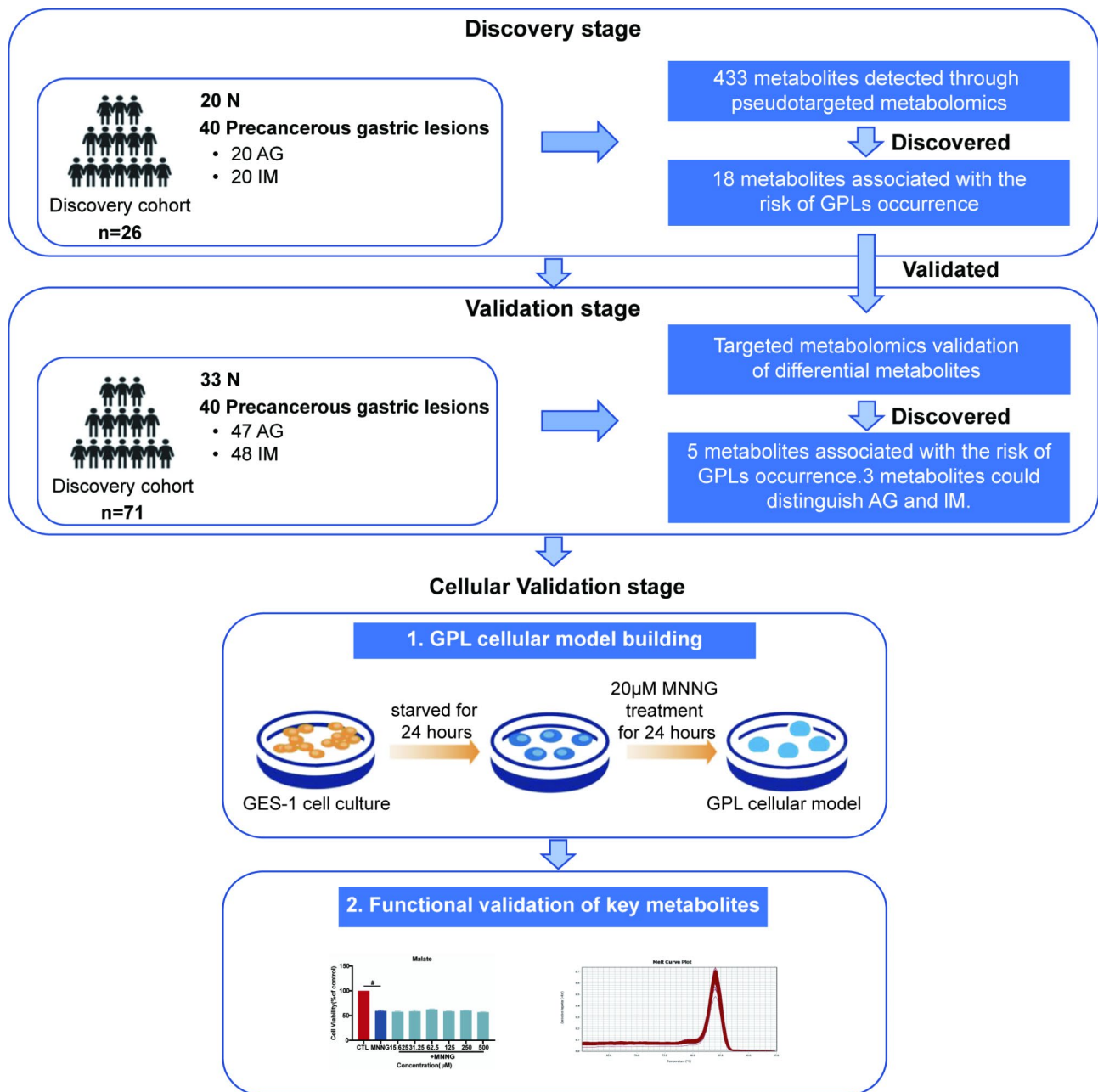


Fig. 1 General workflow of the study. Metabolomics analyses were conducted in two phases involving a total of 97 subjects. Targeted metabolomics validation was performed for five metabolites that were significantly associated with gastric disease progression, and functional validation at the cellular level was performed for three of these metabolites that help to further differentiate between AG and IM tissue

additional 71 patients who required endoscopic examinations (Table 1, Cohort 2) for targeted metabolomics (Fig. 1A). As shown, from absolute targeted metabolomics quantification results, inter-group metabolite variation trends, including glycerophosphocholine, generally matched the relative quantification trends in pseudotargeted metabolomics analysis, indicating that metabolite changes at different disease progression stages were consistent (Figs. 3A–E and 4A–E). Metabolite AUC values in normal and precancerous gastric tissues are shown:

glycerophosphocholine (0.903, 95% CI: 0.834–0.972) (Fig. 4F), tiglylcarnitine (0.779, 95% CI: 0.688–0.870), malate (0.619, 95% CI: 0.512–0.727), sphingosine (0.602, 95% CI: 0.486–0.718), and γ -glutamylglutamic acid (0.643, 95% CI: 0.539–0.746) (Fig. S2A–D), (Supplement Table 6). The aggregated metabolite AUC value was 0.916 (95% CI: 0.851–0.981) (Fig. 4G). These findings demonstrate that glycerophosphocholine, tiglylcarnitine, malate, sphingosine, and γ -glutamylglutamic acid possess the potential to differentiate normal tissues from

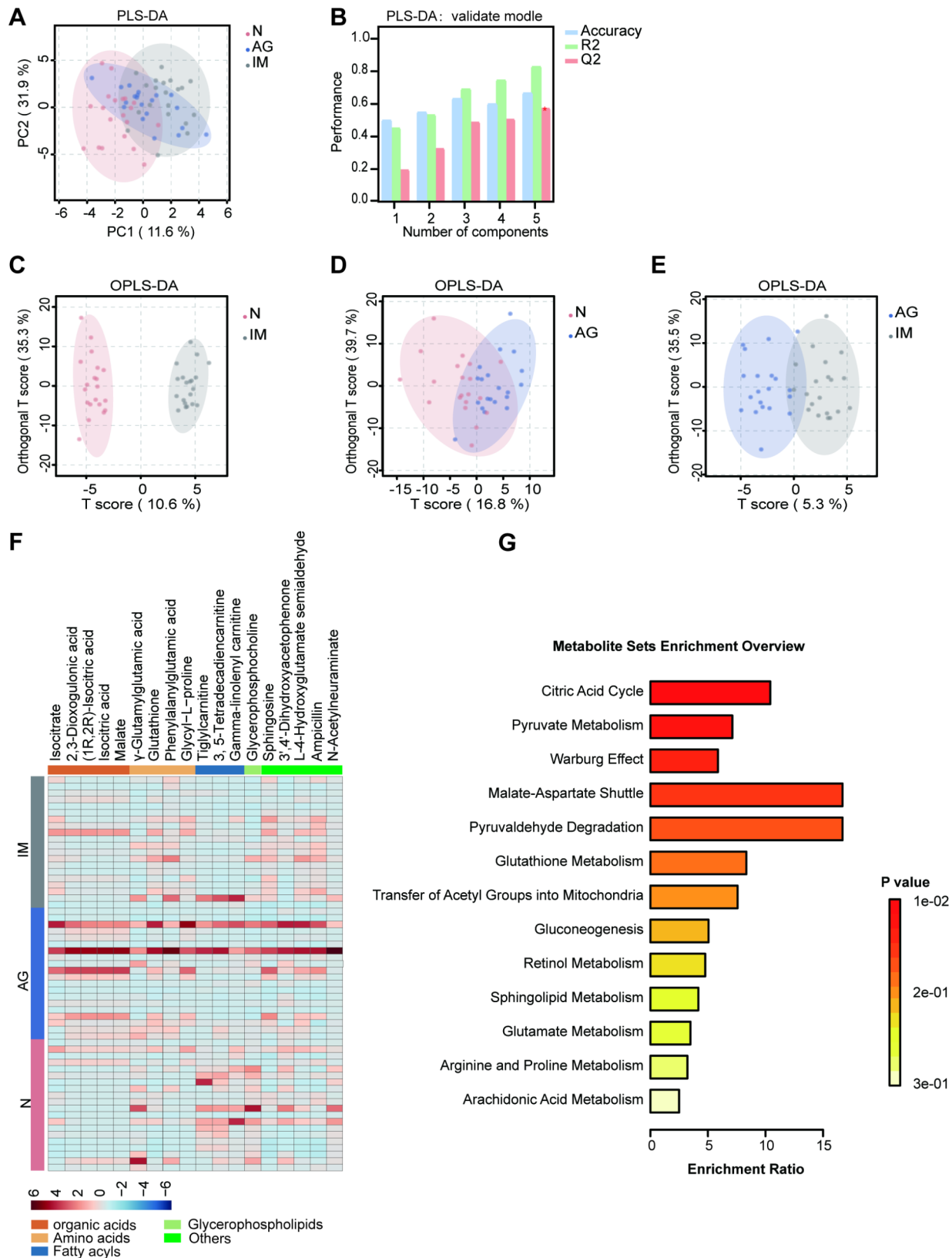


Fig. 2 Metabolic profiling in normal (N) differed when compared with atrophic (AG) and intestinal metaplastic (IM) gastric tissues. **A.** PLS-DA revealed that the N and IM stomach tissues were separated into two distinct clusters, while the AG stomach tissue clusters span between the N and IM clusters. **B.** PLS-DA Modle results showed a valid model. PLS-DA, partial least-squares discriminant analysis. **C–E.** OPLS-DA score plot showed metabolomic differences between N and IM, N and AG, AG and IM. **F.** Heat map showing differential metabolites among N, AG and IM gastric tissues. **G.** Metabolite pathway analysis.

Table 2 Differential metabolite detail parameter table

Description	log ₂ (FC) (N/PLGC)	P	VIP
Isocitrate	-2.0918	0.0211	1.8600
2,3-Dioxogulonic acid	-2.0540	0.0181	1.8398
(1R,2R)-Isocitric acid	-2.0219	0.0350	1.8567
Isocitric acid	-1.8509	0.0326	1.8903
N-acetylneuraminate	-1.2986	0.0000	3.4123
Glutathione	-1.0419	0.0095	1.7107
3,4'-Dihydroxyacetophenone	-0.9588	0.0103	3.0803
γ-Glutamylglutamic acid	-0.8728	0.0061	1.2854
Phenylalanylglutamic acid	-0.8327	0.0167	2.0829
Malate	-0.6988	0.0227	1.3142
L-4-Hydroxyglutamate semialdehyde	-0.6341	0.0263	1.6972
Tiglylcarnitine	0.8597	0.0080	1.6176
Glycyl-L-proline	1.0381	0.0350	2.1572
3, 5-Tetradecadiencarnitine	1.2919	0.0002	2.5105
Sphingosine	1.3201	0.0043	2.3824
Ampicillin	1.4728	0.0375	3.0783
Glycerophosphocholine	1.5106	0.0001	3.1889
Gamma-linolenyl carnitine	1.7009	0.0020	1.8637

precancerous gastric lesions. The combination of these

five metabolites effectively distinguishes normal and precancerous lesion tissues.

Clinically, accurately distinguishing between AG and IM stages has always been a challenge; therefore, we performed ROC curve analysis on AG and IM subgroups in PGLs. Only malate had an AUC value > 0.7, with an AUC of 0.772 (95% CI: 0.671–0.874) (Fig. 4H), while AUC values for glycerophosphocholine and tiglylcarnitine were 0.690 (95% CI: 0.577–0.803) and 0.697 (95% CI: 0.586–0.809), respectively (Fig. S2E–F), (Supplement Table 7). By combining absolute targeted quantification results, malate, glycerophosphocholine, and tiglylcarnitine showed significant differences not only between normal and IM groups, but also between AG and IM groups, suggesting that these metabolites could show potential as biomarkers distinguishing AG and IM tissues.

GPL cell model construction

To create a GPL-related GES-1 cell simulation model (Fig. 1A), GES-1 cells were exposed to 0, 10, 15, 20, 25, 30, 35, and 40 μM MNNG concentrations for 24 h to examine concentration and treatment duration effects. As shown (Fig. 5B), 20 μM MNNG significantly inhibited

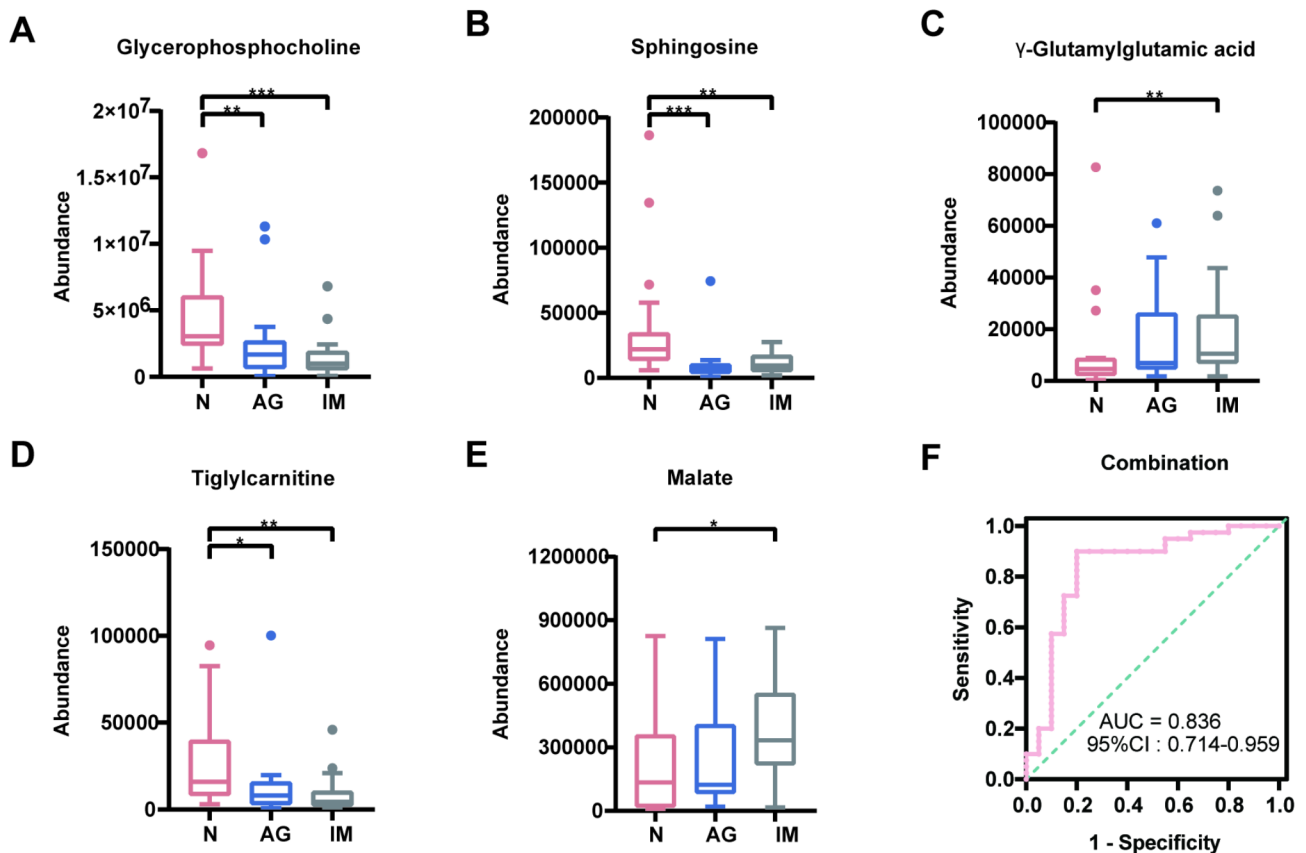


Fig. 3 The identification of metabolite biomarkers, which discriminated N, AG and IM tissues. **A–E.** Among 18 metabolites, five were used to establish standard curves, from which, three showed higher levels in the normal group, while their relative concentrations decreased with disease progression. The other two metabolites showed the opposite trends. **F.** ROC analysis on the five metabolites combination. ROC, receiver operating curve.

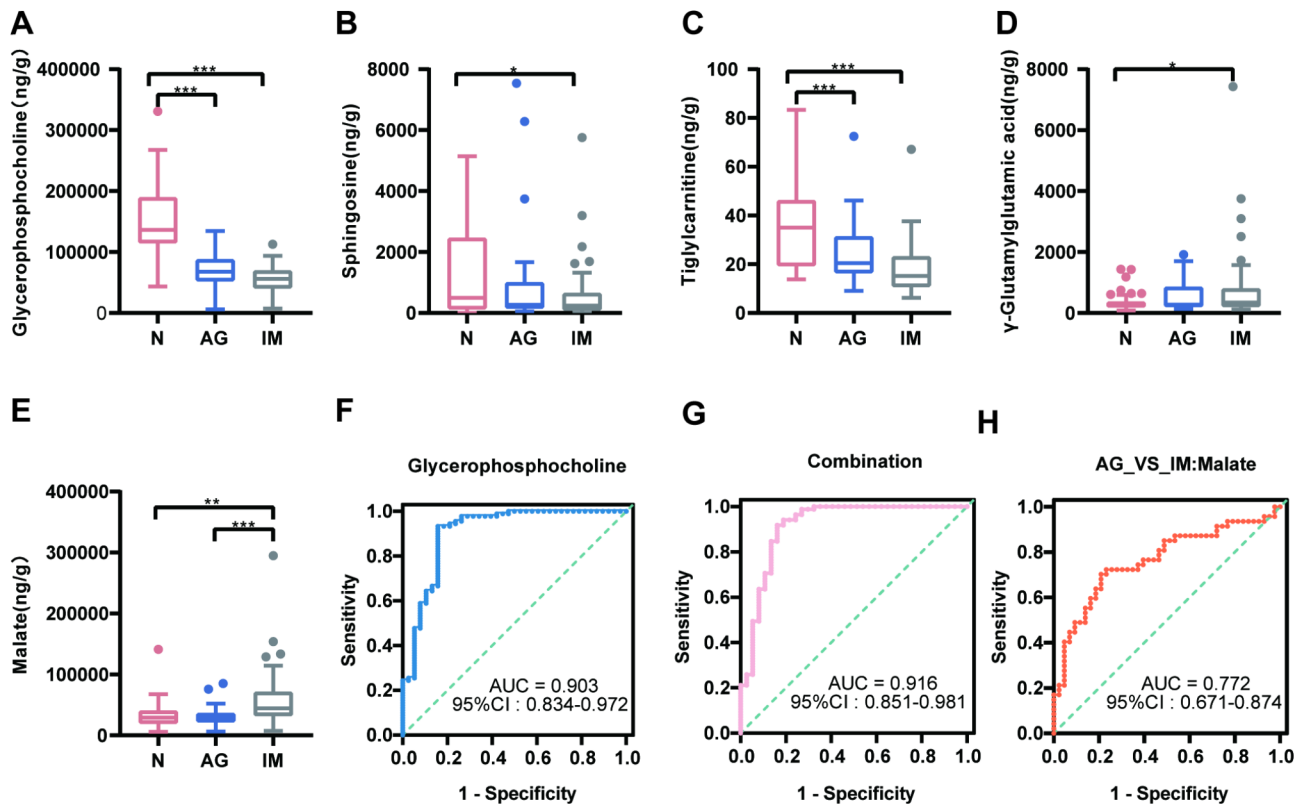


Fig. 4 Metabolite biomarker validation for distinguishing N, AG and IM tissues. **A–E**. The concentrations of the five metabolites in Cohort 2 were compared. **F**. ROC analysis of the glycerophosphocholine. **G**. A ROC combination analysis of the five metabolites. ROC, receiver operating curve. **H**. ROC curves derived from the comparison of malate levels between atrophy and IM groups

GES-1 cell proliferation, leading us to select the 15–25 μ M concentration range, qPCR was then used to evaluate MNNG effects (0, 15, 20, 25 μ M) on intestinalization progression in cells, and after 24 h of 20 μ M treatment, GES-1 cells exhibited significant increases in *CDX2*, *KLF4*, and *MUC2* expression (Fig. 5C–E). *CDX2*, *KLF4*, and *MUC2* are universal indicators of expression when enterocytosis occurs [29]. From analyses, we determined that treating GES-1 cells with 20 μ M MNNG for 24 h optimally induced intestinalization, thereby establishing a GPL cell model.

Key metabolite effects on MNNG-induced GPL

To investigate key metabolite roles and effects on GPL cell model viability following MNNG treatment, cells were starved for 24 h after adherence, pretreated with varying metabolite concentrations for 24 h, and then exposed to MNNG under optimal conditions. As shown (Fig. S3A–C), while metabolites did not significantly impact on cell proliferation, cells pretreated with glycerophosphocholine showed slightly decreased viability at 12.5 μ M, as the concentration of glycerophosphocholine intervention increased, cell viability gradually returned to a level comparable to that of the MNNG modelling group alone. Cells pretreated with 62.5 μ M malate showed

some improvements in viability when compared to the model group, while cells pretreated with 3.125 μ M tiglylcarnitine showed slightly increased viability when compared to the model group, despite CCK8 data showing no significant differences.

Although CCK8 data showing no significant differences, we selected altered concentration gradients for qPCR analyses to explore potential metabolite involvement in gene-level intestinalization processes. We observed that 50 μ M glycerophosphocholine and 3.125 μ M tiglylcarnitine significantly reduced *CDX2* and *KLF4* expression, while 125 μ M malate significantly increased *CDX2* expression (Fig. 6A–C). Although these metabolites did not induce differential *MUC2* expression, as the concentration of malic acid increased, the expression of the *MUC2* gene was observed to increase to a certain extent. Conversely, the intervention of tiglylcarnitine was found to reduce the rise in *MUC2* gene levels to a certain extent (Fig. S4A–C). By combining metabolomics with in vitro data, our findings suggest that glycerophosphocholine and tiglylcarnitine may have the potential to delay intestinalization occurrence and progression in vitro, while malate may promote its development.

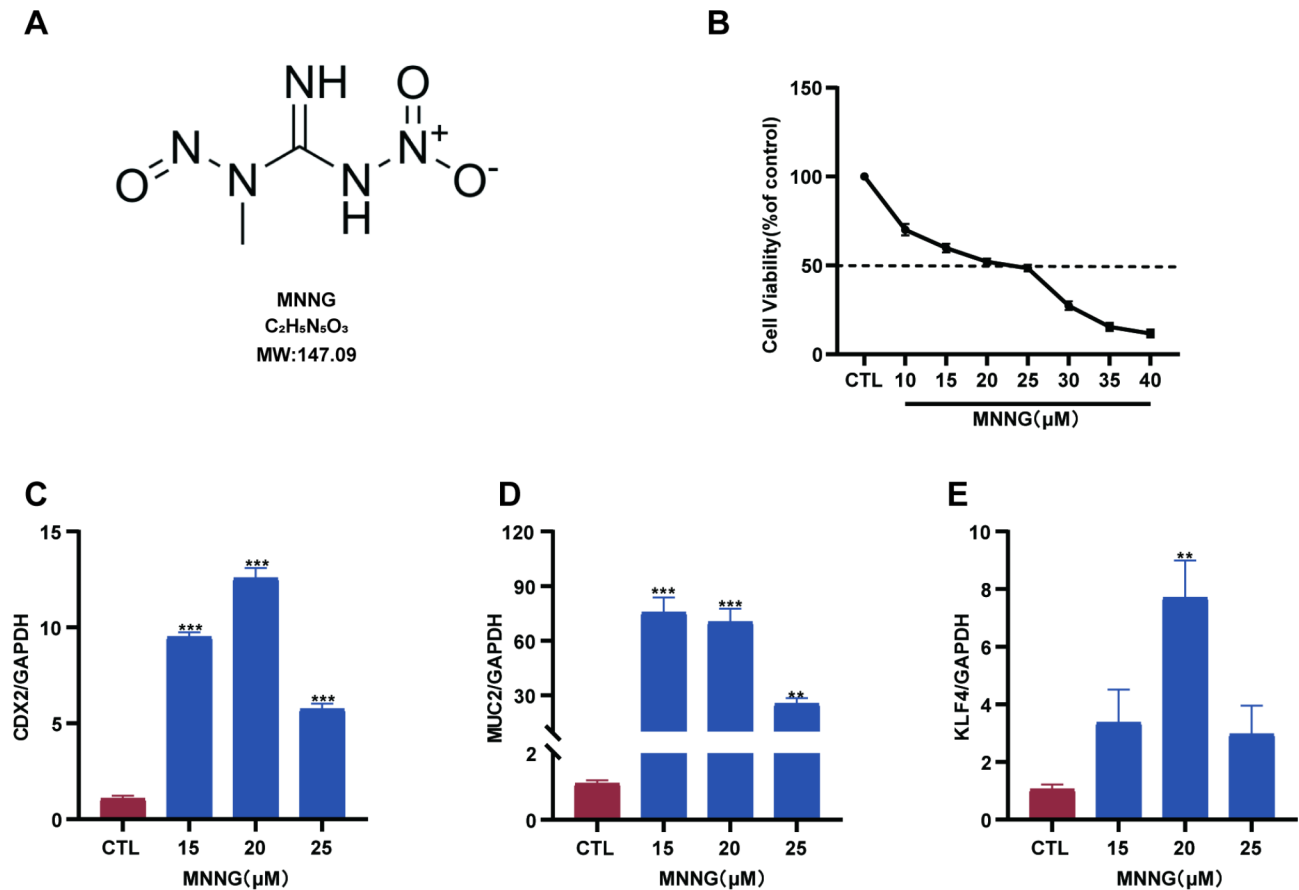


Fig. 5 The construction of a gastric precancerous lesion cell model. **A**. The 1-Methyl-3-nitro-1-nitrosoguanidine (MNNG) chemical structure. **B**. MNNG concentration effects on GES-1 viability. **C–E**. MNNG concentration effects on GES-1 intestinal gene expression. Data are represented by the mean \pm standard error of the mean (SEM). * $p < 0.05$, ** $p < 0.01$ and *** $p < 0.001$ versus the control. All experiments were performed three times and data were normalized to control group data.

Discussion

Metabolomics, as a relatively mature detection technology, has shown significant developmental potential toward gastric diseases and GC at different stages [13, 22]. The metabolites discovered using this approach have shown broad research prospects and clinical applications in disease etiology, early diagnosis, and prognosis [30, 31]. Metabolomics-based analytical techniques have identified distinct and overlapping endogenous biomarkers across different gastric disease stages, encompassing glucose, amino acid, lipid, and nucleotide metabolism pathways. Metabolic alterations have crucial roles in disease onset and progression. However, in studies examining gastric diseases and GC at various stages, metabolic changes have been reported, but the results often vary [22, 23, 32, 33]. Most studies have used easily obtainable samples, such as patient blood, urine, etc., which reflect systemic metabolic changes. In contrast, in our study, we selected gastric tissue samples that more directly reflected metabolic changes at lesion sites. Using advanced metabolomics techniques, we analyzed the

precious and limited gastric tissue samples obtained via endoscopy and have established our own gastric tissue metabolome database, comprising 433 metabolites collected in both positive and negative ion modes.

Using a pseudotargeted metabolomics analysis of the discovery cohort, 18 differential metabolites were identified in both normal and precancerous gastric tissues. ROC curve analysis was then used to identify potential differential metabolites as biomarkers, selecting those with AUC values > 0.7 for validation, and to distinguish between normal and precancerous gastric tissue. For this, we collected a larger validation cohort for absolute targeted quantification analysis. Ultimately, a combination of glycerophosphocholine, tiglylcarnitine, malate, sphingosine, and γ -glutamylglutamic acid potentially acted as powerful biomarkers differentiating normal from precancerous gastric tissue. Moreover, malate, glycerophosphocholine, and tiglylcarnitine effectively differentiated between AG and IM tissue subgroups, suggesting the timely identification and definition of different pathological stages in the gastric Correa cascade process.

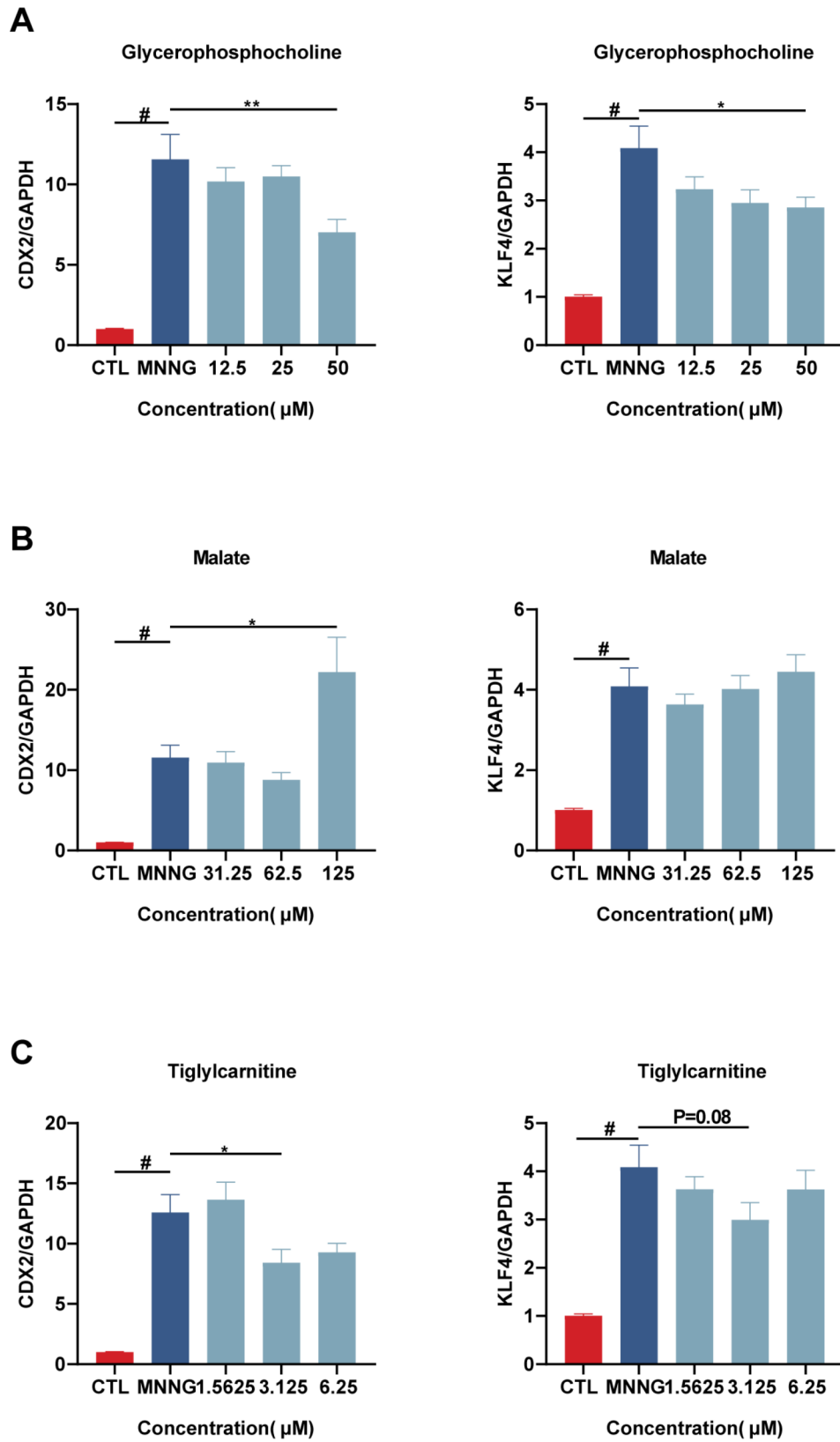


Fig. 6 Pretreatment effects of different metabolite concentrations on IM-related gene (*CDX2* and *KLF4*) expression in a GPL cell model (using GES-1 cells). Data are represented by the mean ± standard error of the mean (SEM). [#]*p* < 0.001, ^{*}*p* < 0.05, and ^{**}*p* < 0.01 versus the control. All experiments were performed three times and data were normalized to control group data.

Glycerophosphocholine can be effectively used to treat and prevent multiple biochemical diseases [34–38]. Other metabolomic studies have shown that glycerophosphocholine levels steadily decrease as GC progresses from gastritis to early GC and then onto advanced GC [24], consistent with our quantitative glycerophosphocholine results across different groups. During the progression from normal gastric tissue to gastric cancer, metabolic reprogramming occurs, including alterations in lipid metabolism. As a type of phospholipid, GPC levels may decrease due to dysregulation in lipid synthesis and degradation. Additionally, the expression levels of phospholipase A2 (PLA2) in gastric cancer tissues are significantly higher than in normal gastric mucosal tissues, and the elevated activity of PLA2 may lead to increased GPC degradation, resulting in reduced GPC levels. Malate is involved in multiple metabolic pathways and is a key intermediate in many biochemical reactions, with important roles in the body. Research has shown that downregulating malate dehydrogenase-3 may advance GC by influencing oxidative stress and stabilizing hypoxia-inducible factor-1 α , with malate, a substrate of this enzyme, crucial in GC progression [39]. Sphingosine is a type of sphingolipid that helps mediate pro-inflammatory events in the gastrointestinal tract via sphingolipid signaling [40]. Previous studies have demonstrated that sphingosine plays a crucial role in apoptosis, inflammatory signaling pathways, and lipid metabolism. Notably, its metabolite sphingosine-1-phosphate (S1P) may have dual effects, either promoting cell survival or accelerating carcinogenesis. Furthermore, the S1P-S1P receptor axis has been reported to be a key player in gastric cancer progression, potentially activating PI3K/Akt, MAPK, and NF- κ B signaling pathways to facilitate gastric epithelial cell proliferation, inhibit apoptosis, and enhance inflammation. Thus, dysregulated sphingosine metabolism may serve as a critical driver of gastric lesion development. Currently, there is limited research on associations between tiglylcarnitine and γ -glutamylglutamic acid and the stomach, thus further exploration and verification studies are required.

As we directly used clinical gastric tissue micro-samples, this approach better reflected metabolic changes at lesion sites when compared to blood, urine, and saliva samples used in previous studies [22–24, 41], maximizing the use of clinical samples and showing potential for translational medicine. We aim to identify potential beneficial metabolites that are abundant in normal tissues but significantly reduced in diseased tissues, with the goal of exploring the protective effects of supplementing these metabolites on the gastric mucosa. Through this approach, we established a gastric tissue metabolic database. By integrating metabolomics analysis of clinical endoscopic biopsy samples with measurements of

glycerophosphocholine, tiglylcarnitine, malate, sphingosine, and γ -glutamylglutamic acid levels, we were able to predict the occurrence of gastric precancerous lesions to a significant extent. Functional validations of these biomarkers were also performed at the cellular level. We showed that glycerophosphocholine, malate, and tiglylcarnitine did not significantly impact GES-1 cell viability under MNNG treatments in our GPL model. However, glycerophosphocholine and tiglylcarnitine partially decreased gene expression related to intestinalization, while malate showed a tendency to enhance this expression.

Our study also has several limitations. First, although the study includes both discovery and validation cohorts, the overall sample size is relatively limited, and the study was conducted at a single center, which may impact the statistical power and generalizability of the findings. Second, the absence of a longitudinal cohort restricts our ability to capture the dynamic evolution of metabolic changes. Third, factors such as *H. pylori* infection, dietary habits, and medication use may influence the gastric tissue metabolome, but these variables were not strictly controlled in our study. To address the above limitations, we plan to expand the sample size in future studies, while strictly controlling for confounding factors such as *H. pylori* infection, diet, and medication use, and simultaneously conducting a longitudinal cohort study. In addition, we plan to adopt a multi-center design in future studies to further validate the robustness and clinical applicability of our results. We also prepare to collect paired tissue and peripheral biofluid samples (such as blood and urine), followed by metabolomics analysis of these samples, aiming to identify more stable and clinically relevant metabolic biomarkers, thereby enabling non-invasive screening and risk assessment. Furthermore, we plan to integrate machine learning and multi-omics approaches to enhance the predictive power of these biomarkers and explore their potential role in the early detection of gastric diseases and personalized medicine.

Conclusions

In summary, we have established the metabolic profiles of clinical precancerous gastric tissue samples for the first time, by focusing on the metabolic changes within the lesions themselves. We identified key metabolite molecules that can distinguish between normal, AG, and IM tissues, which provides new evidence and strategies for clearly defining the precancerous stages and offers a potential approach to distinguishing the pathological stages of AG and IM. However, further research is needed, including expanding the cohort, assessing the consistency of metabolic changes in different matrices, and conducting animal experiments to explore mechanisms and clinical applications.

Abbreviations

AG	Atrophic gastritis
AUC	Area under the curve
CCK8	Cell counting kit-8
CI	Confidence interval
FBS	Fetal bovine serum
FC	Fold change
GC	Gastric cancer
GPL	Gastric precancerous lesions
IM	Intestinal metaplasia
MNNG	1-methyl-3-nitro-1-nitrosoguanidine
OPLS-DA	Orthogonal partial least squares discriminant analysis
PLS-DA	Partial least squares discriminant analysis
qRT-PCR	Quantitative real time PCR
ROC	Receiver operating characteristic
UPLC-MS/MS	Ultra-Performance Liquid Chromatography-Tandem Quadrupole Mass Spectrometry
VIP	Variable importance in the projection.

Supplementary Information

The online version contains supplementary material available at <https://doi.org/10.1186/s12876-025-03898-9>.

Supplementary Material 1
Supplementary Material 2
Supplementary Material 3
Supplementary Material 4
Supplementary Material 5
Supplementary Material 6
Supplementary Material 7

Acknowledgements

We would like to thank all participants in this study.

Author contributions

Y.X. and Y.R. designed the study. X.Z, Z.L, B.J, C.M: performed experiments and collected the data. X.Z, B.X, Y.G, Y.S, Y.D: analyzed the data. X.Z, Z.L: draw the figures and wrote the original manuscript, Y.R: revised the manuscript.

Funding

This work was supported by a grant from the National Natural Science Foundation of China (Grant No. 32101964, 32372302, 82405210), China Postdoctoral Science Foundation (Grant No. 2023M731346); the Natural Science Foundation of Jiangsu Province (BK20241755); Top Talent Support Program for young and middle-aged people of Wuxi Health Committee (Grant No. BJ2023046); Wuxi Taihu Lake Talent Plan, Supports for Leading Talents in Medical and Health Profession.

Data availability

Data and software availability pseudotargeted metabolomics data on gastric have been deposited in the European Bioinformatics Institute under accession code MTBLS11835. Data is provided within the manuscript and related files at the same time.

Ethics declarations

Ethics approval and consent to participate

This retrospective study was approved by the Ethics Committee of Affiliated Hospital of Jiangnan University and conducted according to the principles of the Declaration of Helsinki (approved No. of ethic committee: LS2024300). All patients provided written informed consent before enrollment.

Consent for publication

Not Applicable.

Competing interests

The authors declare no competing interests.

Conflict of interest

The authors declare no conflicts of interest.

Received: 6 January 2025 / Accepted: 15 April 2025

Published online: 29 April 2025

References

1. Thrift AP, Wenker TN, El-Serag HB. Global burden of gastric cancer: epidemiological trends, risk factors, screening and prevention. *Nat Reviews Clin Oncol*. 2023;20(5):338–49.
2. Zong L, Abe M, Seto Y, Ji J. The challenge of screening for early gastric cancer in China. *Lancet (London England)*. 2016;388(10060):2606.
3. Correa P. Human gastric carcinogenesis: a multistep and multifactorial process—first American Cancer society award lecture on cancer epidemiology and prevention. *Cancer Res*. 1992;52(24):6735–40.
4. You WC, Li JY, Blot WJ, Chang YS, Jin ML, Gail MH, Zhang L, Liu WD, Ma JL, Hu YR. Evolution of precancerous lesions in a rural Chinese population at high risk of gastric cancer. *Int J Cancer*. 1999;83(5):615–9.
5. Sipponen P, Maarros H-I. Chronic gastritis. *Scand J Gastroenterol*. 2015;50(6):657–67.
6. de Vries AC, van Grieken NC, Looman CW, Casparie MK, de Vries E, Meijer GA, Kuipers EJ. Gastric cancer risk in patients with premalignant gastric lesions: a nationwide cohort study in the Netherlands. *Gastroenterology*. 2008;134(4):945–52.
7. den Hoed CM, Holster IL, Capelle LG, de Vries AC, den Hartog B, ter Borg F, Biermann K, Kuipers EJ. Follow-up of premalignant lesions in patients at risk for progression to gastric cancer. *Endoscopy*. 2013;45(04):249–56.
8. Salvatori S, Marafini I, Laudisi F, Monteleone G, Stolfi C. *Helicobacter pylori* and gastric cancer: pathogenetic mechanisms. *Int J Mol Sci*. 2023;24(3):2895.
9. Malfertheiner P, Camargo MC, El-Omar E, Liou J-M, Peek R, Schulz C, Smith SJ, Suerbaum S. *Helicobacter pylori* infection. *Nat Reviews Disease Primers*. 2023;9(1):19.
10. Hanahan D. RA Weinberg 2011 Hallmarks of cancer: the next generation. *Cell*. 144 5 646–74.
11. Ward PS, Thompson CB. Metabolic reprogramming: a cancer hallmark even Warburg did not anticipate. *Cancer Cell*. 2012;21(3):297–308.
12. Pearce EL, Poffenberger MC, Chang C-H, Jones RG. Fueling immunity: insights into metabolism and lymphocyte function. *Science*. 2013;342(6155):1242454.
13. Xiao S, Zhou L. Gastric cancer: metabolic and metabolomics perspectives. *Int J Oncol*. 2017;51(1):5–17.
14. Abbassi-Ghadi N, Kumar S, Huang J, Goldin R, Takats Z, Hanna G. Metabolomic profiling of oesophago-gastric cancer: a systematic review. *Eur J Cancer*. 2013;49(17):3625–37.
15. Huang S, Guo Y, Li Z, Zhang Y, Zhou T, You W, Pan K, Li W. A systematic review of metabolomic profiling of gastric cancer and esophageal cancer. *Cancer Biology Med*. 2020;17(1):181.
16. Jayavelu ND, Bar NS. Metabolomic studies of human gastric cancer. *World J Gastroenterology: WJG*. 2014;20(25):8092.
17. Nicholson JK, Lindon JC. *Metabonomics Nat*. 2008;455(7216):1054–6.
18. Holmes E, Wilson ID, Nicholson JK. Metabolic phenotyping in health and disease. *Cell*. 2008;134(5):714–7.
19. Rochfort S. Metabolomics reviewed: a new omics platform technology for systems biology and implications for natural products research. *J Nat Prod*. 2005;68(12):1813–20.
20. Wang J, Kunzke T, Prade VM, Shen J, Buck A, Feuchtinger A, Haffner I, Luber B, Liu DH, Langer R. Spatial metabolomics identifies distinct tumor-specific subtypes in gastric cancer patients. *Clin Cancer Res*. 2022;28(13):2865–77.
21. Kuligowski J, Sanjuan-Herraez D, Vazquez-Sanchez MA, Brunet-Vega A, Pericay C, Ramirez-Lázaro MJ, Lario S, Gombau L, Junquera F, Calvet X. Metabolomic analysis of gastric cancer progression within the Correa's cascade using ultraperformance liquid chromatography–mass spectrometry. *J Proteome Res*. 2016;15(8):2729–38.
22. Huang S, Guo Y, Li Z-W, Shui G, Tian H, Li B-W, Kadeerhan G, Li Z-X, Li X, Zhang Y. Identification and validation of plasma metabolomic signatures in precancerous gastric lesions that progress to cancer. *JAMA Netw Open*. 2021;4(6):e2114186–2114186.

23. Yu L, Lai Q, Feng Q, Li Y, Feng J, Xu B. Serum metabolic profiling analysis of chronic gastritis and gastric cancer by untargeted metabolomics. *Front Oncol.* 2021;11:636917.
24. Chan AW, Mercier P, Schiller D, Bailey R, Robbins S, Eurich DT, Sawyer MB, Broadhurst D. 1H-NMR urinary metabolomic profiling for diagnosis of gastric cancer. *Br J Cancer.* 2016;114(1):59–62.
25. Zheng F, Zhao X, Zeng Z, Wang L, Lv W, Wang Q, Xu G. Development of a plasma pseudotargeted metabolomics method based on ultra-high-performance liquid chromatography–mass spectrometry. *Nat Protoc.* 2020;1–19.
26. Wang X, Zhang S, Chua EG, He Y, Li X, Liu A, Chen H, Wise MJ, Marshall BJ, Sun D. A re-testing range is recommended for 13 C-and 14 C-urea breath tests for *Helicobacter pylori* infection in China. *Gut Pathogens.* 2021;13(1):38.
27. Ren Y, Geng Y, Du Y, Li W, Lu Z-M, Xu H-Y, Xu G-H, Shi J-S, Xu Z-H. Polysaccharide of *hericium erinaceus* attenuates colitis in C57BL/6 mice via regulation of oxidative stress, inflammation-related signaling pathways and modulating the composition of the gut microbiota. *J Nutr Biochem.* 2018;57:67–76.
28. Ren Y, Sun Q, Gao R, Sheng Y, Guan T, Li W, Zhou L, Liu C, Li H, Lu Z et al. Low weight polysaccharide of *hericium erinaceus* ameliorates colitis via inhibiting the NLRP3 inflammasome activation in association with gut microbiota modulation. *Nutrients* 2023, 15(3).
29. Tong Q-Y, Pang M-J, Hu X-H, Huang X-Z, Sun J-X, Wang X-Y, Burclaff J, Mills JC, Wang Z-N, Miao Z-F. Gastric intestinal metaplasia: progress and remaining challenges. *J Gastroenterol.* 2024;59(4):285–301.
30. Matsuoka T, Yashiro M. Bioinformatics analysis and validation of potential markers associated with prediction and prognosis of gastric Cancer. *Int J Mol Sci.* 2024;25(11):5880.
31. Lei C, Gong D, Zhuang B, Zhang Z. Alterations in the gastric microbiota and metabolites in gastric cancer: an update review. *Front Oncol.* 2022;12:960281.
32. Mu X, Ji C, Wang Q, Liu K, Hao X, Zhang G, Shi X, Zhang Y, Gonzalez FJ, Wang Q. Non-targeted metabolomics reveals diagnostic biomarker in the tongue coating of patients with chronic gastritis. *J Pharm Biomed Anal.* 2019;174:541–51.
33. Cui J, Liu Y, Hu Y, Tong J, Li A, Qu T, Qin X, Du G. NMR-based metabolomics and correlation analysis reveal potential biomarkers associated with chronic atrophic gastritis. *J Pharm Biomed Anal.* 2017;132:77–86.
34. Barbagallo M, Giordano M, Meli M, Panzarasa R. alpha-Glycerophosphocholine in the mental recovery of cerebral ischemic attacks. An Italian multicenter clinical trial. *Ann NY Acad Sci.* 1994;717:253–69.
35. Lee SH, Choi BY, Kim JH, Kho AR, Sohn M, Song HK, Choi HC, Suh SW. Late treatment with choline alfoscerate (l-alpha glycerylphosphorylcholine, alpha-GPC) increases hippocampal neurogenesis and provides protection against seizure-induced neuronal death and cognitive impairment. *Brain Res.* 2017;1654:66–76.
36. Drago F, Mauceri F, Nardo L, Valerio C, Lauria N, Rampello L, Guidi G. Behavioral effects of L-alpha-glycerylphosphorylcholine: influence on cognitive mechanisms in the rat. *Pharmacol Biochem Behav.* 1992;41(2):445–8.
37. Na G, Kwak SH, Jang SH, Noh HE, Kim J, Yang S, Jung J. Supplementary effect of choline alfoscerate on speech recognition in patients with age-related hearing loss: A prospective study in 34 patients (57 ears). *Front Aging Neurosci.* 2021;13:684519.
38. Choi JJ, Hwang JS, Shin YJ. Effect of oral choline alfoscerate on patients with keratoconjunctivitis Sicca. *Nutrients.* 2020;12(5):1526.
39. Huang Y, Yang Y, Chen X, Zeng S, Chen Y, Wang H, Lv X, Hu X, Teng L. Down-regulation of malic enzyme 3 facilitates progression of gastric carcinoma via regulating intracellular oxidative stress and hypoxia-inducible factor-1 α stabilization. *Cell Mol Life Sci.* 2024;81(1):375.
40. Sukocheva OA, Furuya H, Ng ML, Friedemann M, Menschikowski M, Tarasov VV, Chubarev VN, Klochkov SG, Neganova ME, Mangoni AA. Sphingosine kinase and sphingosine-1-phosphate receptor signaling pathway in inflammatory Gastrointestinal disease and cancers: A novel therapeutic target. *Pharmacol Ther.* 2020;207:107464.
41. Kaźmierczak-Siedlecka K, Muszyński D, Styburski D, Makarewicz J, Sobocki BK, Ulański P, Połom K, Stachowska E, Skonieczna-Żydecka K, Kalinowski L. Untargeted metabolomics in gastric and colorectal cancer patients—preliminary results. *Front Cell Infect Microbiol.* 2024;14:1394038.

Publisher's note

Springer Nature remains neutral with regard to jurisdictional claims in published maps and institutional affiliations.